The Journal of Infectious Diseases

SUPPLEMENT ARTICLE

Griffithsin Inhibits Nipah Virus Entry and Fusion and Can Protect Syrian Golden Hamsters From Lethal Nipah Virus Challenge

Michael K. Lo,[1] Jessica R. Spengler,[1] Lauren R. H. Krumpe,[2] Stephen R. Welch,[1] Anasuya Chattopadhyay,[3] Jessica R. Harmon,[1] JoAnn D. Coleman-McCray,[1] Florine E. M. Scholte,[1] Anne L. Hotard,[1] Joshua L. Fuqua,[4] John K. Rose,[3] Stuart T. Nichol,[1] Kenneth E. Palmer,[4] Barry R. O'Keefe,[5,6] and Christina F. Spiropoulou[1]

[1]Viral Special Pathogens Branch, Division of High-Consequence Pathogens and Pathology, National Center for Emerging and Zoonotic Infectious Diseases, Centers for Disease Control and Prevention, Atlanta, Georgia, USA, [2]Basic Science Program, Frederick National Laboratory for Cancer Research, Frederick, Maryland, USA, [3]Yale University School of Medicine, New Haven, Connecticut, USA, [4] Center for Predictive Medicine for Biodefense and Emerging Infectious Diseases, University of Louisville School of Medicine, Louisville, Kentucky, USA, [5]Molecular Targets Program, Center for Cancer Research, National Cancer Institute, Frederick, Maryland, USA, [6]Natural Products Branch, Developmental Therapeutics Program, Division of Cancer Treatment and Diagnosis, National Cancer Institute, Frederick, Maryland, USA

Nipah virus (NiV) is a highly pathogenic zoonotic paramyxovirus that causes fatal encephalitis and respiratory disease in humans. There is currently no approved therapeutic for human use against NiV infection. Griffithsin (GRFT) is high-mannose oligosaccharide binding lectin that has shown in vivo broad-spectrum activity against viruses, including severe acute respiratory syndrome coronavirus, human immunodeficiency virus 1, hepatitis C virus, and Japanese encephalitis virus. In this study, we evaluated the in vitro antiviral activities of GRFT and its synthetic trimeric tandemer (3mG) against NiV and other viruses from 4 virus families. The 3mG had comparatively greater potency than GRFT against NiV due to its enhanced ability to block NiV glycoprotein-induced syncytia formation. Our initial in vivo prophylactic evaluation of an oxidation-resistant GRFT (Q-GRFT) showed significant protection against lethal NiV challenge in Syrian golden hamsters. Our results warrant further development of Q-GRFT and 3mG as potential NiV therapeutics.

Keywords. antiviral; Griffithsin; hamster; Nipah; therapeutic.

Nipah virus (NiV) is a zoonotic henipavirus harbored by pteropid bats, and it is responsible for causing near-annual outbreaks of fatal human encephalitis and respiratory disease in Bangladesh and India [1]. Although several therapeutics protect against lethal NiV challenge in animals [2–4], none is currently approved for human use. Inhibitors of NiV entry and spread generally target protein interactions involved in receptor binding or membrane fusion processes [5–10], but the glycosylation of NiV glycoproteins presents another viable target for therapeutic development [11–13]. Griffithsin (GRFT) is a homodimeric high-mannose oligosaccharide binding lectin currently being evaluated in clinical trials as a topical microbicide against human immunodeficiency virus 1 (HIV-1) [14, 15], and it has also demonstrated in vivo broad-spectrum activity against viruses including severe acute respiratory syndrome coronavirus, hepatitis C virus, and Japanese encephalitis virus [16–19]. In this study, we characterized the in vitro antiviral activities of GRFT and its synthetic trimeric tandemer (3mG) [20] against NiV and other viruses from 4 virus families, and tested the in vivo prophylactic potential of 3mG and an oxidation-resistant form of GRFT (Q-GRFT) against lethal NiV challenge in the Syrian golden hamster model. Our results warrant further development of Q-GRFT and 3mG as potential NiV therapeutics.

MATERIALS AND METHODS

Biosafety

All work with infectious virus or infected animals was conducted in a biosafety level 4 (BSL-4) laboratory at the Centers for Disease Control and Prevention (CDC) following established BSL-4 standard operating procedures approved by the Institutional Biosafety Committee.

Compounds and Plasmids

GRFT, monomeric GRFT (mGRFT), mGRFT tandemers, and Q-GRFT were expressed and purified as described previously [20–23]. Codon-optimized mCherry, Malaysian NiV-F, and NiV-G coding sequences were synthesized and cloned into pCAGGS expression plasmids (GenScript). A pTM1-based plasmid encoding enhanced green fluorescent protein (eGFP) under the control of a T7 polymerase promoter (pT7-eGFP)

Presented in part: International Union of Microbiological Sciences 2017, Singapore; International Conference for Antiviral Research 2017, Atlanta; Viruses and Cells Gordon Research Conference 2019, Italy.

Correspondence: C. F. Spiropoulou, PhD, Centers for Disease Control and Prevention, 1600 Clifton Road, Mailstop G-14, Atlanta, GA 30329 (ccs8@cdc.gov).

The Journal of Infectious Diseases® 2020;221(S4):S480–92

DOI: 10.1093/infdis/jiz630

was a gift from Dr. Mark E. Peeples (The Research Institute at Nationwide Children's Hospital).

Cells and Viruses

HeLa, HEK293T/17, HT-1080, Vero, Huh7, and BSRT7/5 cells [24] were cultivated as previously described [25, 26]. CHO-K1 cells were maintained in F-12K medium supplemented with 10% fetal bovine serum. All cells were incubated at 37°C in 5% CO_2. Wild-type NiVs (NiV Malaysia [NiV-M], NiV Bangladesh [NiV-B]), Hendra virus (HeV), recombinant reporter NiVs (rNiV-RLuc [formerly named NiV-Luc2AM], rNiV-ZsG [formerly named NiV-GFP2AM]) [27], measles vaccine virus ($rMV^{EZ}EGFP(3)$) [28], mumps virus (rMuV-EGFP, Iowa 2006 strain) [29], human parainfluenza virus 3 (hPIV3-GFP, JS strain) [30], human metapneumovirus (hMPV-GFP, CAN97-83 strain) [31], Lassa virus (rLASV-ZsG) [32], and Crimean-Congo hemorrhagic fever virus (rCCHFV-ZsG) [33] were propagated in Vero-E6, Vero, or Huh7 cells and were quantitated by 50% tissue culture infectious dose ($TCID_{50}$) assay [34]. Unless stated otherwise, all infections were performed at multiplicity of infection of 0.25.

Reporter Virus and Minigenome Assays

Recombinant reporter virus assays were performed as previously described [27, 35]. In brief, 10^4 cells pretreated with serial dilutions of GRFT for 1 hour were infected with the above-mentioned reporter viruses (without washing) for 24–72 hours and then assayed either for GFP, GFP + cells, or for *Renilla* luciferase activity. A nanoluciferase (NLuc)-based NiV minigenome assay was conducted as previously described [25]. A total of 10^4 BSRT7/5 cells [24] (per well) were transfected using LT-1 transfection reagent (Mirus Bio) with appropriate amounts of NiV support plasmids (see Supplemental Methods for details). Compounds were added directly to the media 4 hours posttransfection, and at 48 hours NLuc activity was measured.

Virus Yield Reduction and Immune Fluorescence Assays

A total of 10^4 cells infected with NiV-M, NiV-B, or rNiV-ZsG for 1 hour were washed and treated with GRFT or 3mG. At 24–48 hours post infection (hpi), viral titers from supernatants were quantitated by $TCID_{50}$ assay. Fluorescent micrographs of rNiV-ZsG-infected cells were captured using the EVOS FL Cell Imaging System (Thermo Fisher Scientific) at ×4 magnification. For immune fluorescence, infected cells were fixed in 10% formalin, stained using GRFT at 1 μg/mL and a monoclonal anti-NiV nucleoprotein antibody [36], followed by staining with anti-GRFT polyclonal rabbit antibody, and then detected with anti-rabbit Dylight488 and antimouse Dylight550 antibodies (1:1000 dilution; Bethyl Laboratories) along with 4′,6-diamidino-2-phenylindole (DAPI) nuclear stain (1:1000 dilution). Fluorescence micrographs were taken using a Nikon Axioscope Ti inverted fluorescence microscope at ×4 magnification.

NiV-F and NiV-G Glycoprotein Expression, Purification, and Detection

HEK293T/17 cells (3×10^5) were transfected with 3 μg of NiV-F AU1, NiV-G His6×, or mCherry plasmid. At 48 hours post transfection, cells were harvested in 250 μL radioimmunoprecipitation buffer/well (Thermo Fisher Scientific). NiV-F AU1 was purified from cell lysates using an anti-AU1 affinity bead column according to the manufacturer's recommendations (BioLegend). NiV-G His6× was purified using nickel-nitrilotriacetic acid affinity resin. Cell lysates and purified proteins were run on SDS-PAGE gels (Supplemental Figure 1A), transferred onto polyvinylidene difluoride membranes, and probed with either anti-AU1 (Bethyl) or anti-6His6× (Cell Signaling Technology) rabbit antibodies, or with GRFT along with anti-GRFT polyclonal rabbit sera, and detected using goat anti-rabbit 680RD secondary antibodies (LI-COR) (Supplemental Figure 1B and C). Protein bands were visualized using LI-COR imaging.

Enzyme-Linked Immunosorbent Assay Against Purified NiV-F and NiV-G Glycoproteins

GRFT binding enzyme-linked immunosorbent assays (ELISAs) were performed as previously described [15]. In brief, 1 picomole (or 50 ng) of purified NiV-F AU1 or NiV-G His6× was bound to a 96-well plate, which was washed and blocked with bovine serum albumin. Between requisite washing steps, plates were incubated with increasing amounts of GRFT or 3mG, followed by incubation with a 1:1000 dilution of the anti-GRFT rabbit polyclonal antibody preparation. The bound GRFT was determined using goat anti-rabbit antibodies conjugated to horseradish peroxidase (HRP) and a TMB peroxidase substrate system. Peroxidase activity was quenched using 1 M hydrochloric acid and absorbance was measured at 450 nm. Additional details are found in the Supplemental Methods.

Pseudotyped Vesicular Stomatitis Virus Entry Assay

A replication-deficient vesicular stomatitis virus (VSV) expressing eGFP in place of the VSV attachment glycoprotein (VSV-ΔG-eGFP) was pseudotyped with either VSV G (VSVpt) or NiV-F and NiV-G glycoproteins (NiVpt) as previously described [37]. Fifty particles of VSVpt or NiVpt were used to either infect Vero cells in conjunction with GRFT/3mG treatment for 24 hours or to infect Vero cells that were pretreated with GRFT/3mG for 1 hours and then removed before infection. At 24 hpi, numbers of eGFP expressing cells were visualized and counted [37].

Cytopathic Effect Inhibition Assays

Inhibition of virus-induced cytopathic effect (CPE) was assayed as previously described using CellTiter-Glo 2.0 reagent (Promega) in a BioTek HD1 Synergy plate reader [25]. Luminescence values were normalized to uninfected cell controls according to % viability as follows: % viability = [(specific value-reference value)/

(dimethyl sulfoxide control value – reference value)] × 100. Reference values were derived from control wells without cells. Uninfected cell control viability values (after subtraction of reference values) were set at 100% inhibition of CPE.

Qualitative and Quantitative Fusion Assays

A total of 10^4 HT-1080 cells were transfected for 4 hours with 0.1 μg each of NiV-F AU1 and NiV-G HA expression plasmids, washed, and replenished with growth media containing GRFT or 3mG. At 24 hours post transfection, cells were stained using CellMask Green (Thermo Fisher Scientific) and DAPI and viewed using a Nikon Axioscope Ti inverted fluorescence microscope at ×4 magnification. For quantitative fusion assay, 2×10^4 CHO-K1 cells were transfected for 4 hours with 0.1 μg each of NiV-F AU1, NiV-G HA, and pT7-eEGFP plasmids. Negative control CHO-K1 cells were transfected with 0.2 μg of NiV-F AU1 and 0.1 μg of pT7-eGFP. Cells then were washed and replenished with growth media containing GRFT or 3mG. BSRT7/5 cells (2×10^4) were then overlaid onto CHO-K1 cells. At ~16 hours postoverlay, green fluorescent NiV glycoprotein-induced syncytia were visualized at ×2.5 magnification on a Cytation5 instrument (BioTek) and counted from photograph montages of each well using Gen5 Software. Fluorescent objects that were both >75 μm in diameter and had a fluorescence reading >5000 were classified as positive syncytia. Additional details are found in the Supplemental Methods.

Ethics Statement and Animals

All animal experiments were approved by the CDC Institutional Animal Care and Use Committee and performed in an AAALAC-International approved facility. Groups of 5–10 female HsdHan:AURA golden Syrian hamsters (6 weeks of age; Envigo no. 8903F) were inoculated intranasally (IN) with Dulbecco's modified Eagle's medium or NiV-B (10^7 $TCID_{50}$). On 1 and 2 days post infection (dpi) and/or -1 and -2 dpi, animals were treated IN with vehicle control (phosphate-buffered saline [PBS]), GRFT (10 mg/kg), or 3mG (10 mg/kg). Hamsters were humanely euthanized with isoflurane vapor when they met euthanasia criteria or at the completion of the study (28 dpi). Additional clinical scoring details are found in the Supplementary Methods.

Quantitative Reverse-Transcription Polymerase Chain Reaction

RNA was extracted from blood and homogenized tissue samples using the MagMAX-96 Total RNA Isolation Kit (Thermo Fisher Scientific) on a 96-well ABI MagMAX extraction platform with a DNaseI treatment step according to manufacturer's instructions. The RNA was quantitated using one-step real-time reverse-transcription polymerase chain reaction (qRT-PCR) targeting the N gene sequence [38] and was standardized to 18S ribosomal RNA with a SuperScript III Platinum One-Step qRT-PCR Kit (Thermo Fisher Scientific) according to manufacturer's instructions.

Plasma Antibody Analysis

Total NiV-specific immunoglobulin G (IgG) and neutralizing antibodies were measured as previously described [2]. Gamma-irradiated plasma were serially diluted 1:100, 1:400, 1:1600, and 1:6400 and incubated for 1 hour on plates coated with inactivated NiV lysate or Vero cell control lysate at 37°C. With requisite washing steps, plates were then incubated with antibody detector protein A/G conjugated with HRP (Thermo Fisher Scientific) for 1 hour at 37°C, followed by incubation with ABTS substrate (KPL) for one-half hour at 37°C. Absorbance was read at 410 nm and 490 nm. Well-specific 490 nm absorbance values were subtracted from their corresponding 410 nm values. The resulting values from Vero control lysates were then subtracted from those taken from NiV-infected lysates. Cutoff values were derived from adding the mean of 6 negative control plasma to 3 times the standard deviation of the mean. Samples were considered true IgG positives if their values were above cutoff values for both 1:100 and 1:400 dilutions. Additional details are found in the Supplementary Methods. Two-fold dilutions of plasma were incubated with 200 $TCID_{50}$ of NiV-B in duplicate for 1 hour and then transferred onto Vero cells for 6 days at 37°C. Neutralizing titers were recorded as the lowest reciprocal dilution at which all wells lacked CPE.

Statistical Analyses

All statistical analyses were performed using GraphPad Prism 8.1.2. Animal survival was analyzed by log-rank (Mantel-Cox) and Gehan-Breslow-Wilcoxon test. Quantitative fusion assay and virus yield comparisons between GRFT and 3mG were analyzed using multiple *t* tests with adjusted *P* values. Fifty percent effective concentrations and 50% cytotoxic concentrations were calculated using 4-parameter variable slope nonlinear regression fitting of mean values of all antiviral assays.

RESULTS

GRFT Inhibits NiV Reporter Gene Expression and Infectious Virus Production, but Not Viral RNA Transcription or Replication

We initially tested GRFT against a reporter NiV expressing *Renilla* luciferase (rNiV-RLuc) [27]. Pretreatment of 4 different cell lines with increasing amounts of GRFT 1 hour before rNiV-RLuc infection resulted in dose-dependent decreases in reporter activity assayed at 24 hpi, with 50% effective inhibitory concentration (EC_{50}) values ranging between 0.5 and 1.5 μg/mL (~20–60 nM) (Figure 1A, Table 1). We then measured wild-type recombinant NiV (rNiV) infectious virus yield at 24 hpi from cells treated with GRFT immediately after infection and observed a dose-dependent decrease >2 $\log_{10}$ $TCID_{50}$ (Figure 1B). To determine whether GRFT interferes with NiV replication directly at the level of RNA transcription and replication, we tested increasing concentrations of GRFT against a reporter NiV minigenome expressing NLuc and observed no inhibition of reporter signal, consistent with no direct inhibition of viral RNA levels (Figure 1C).

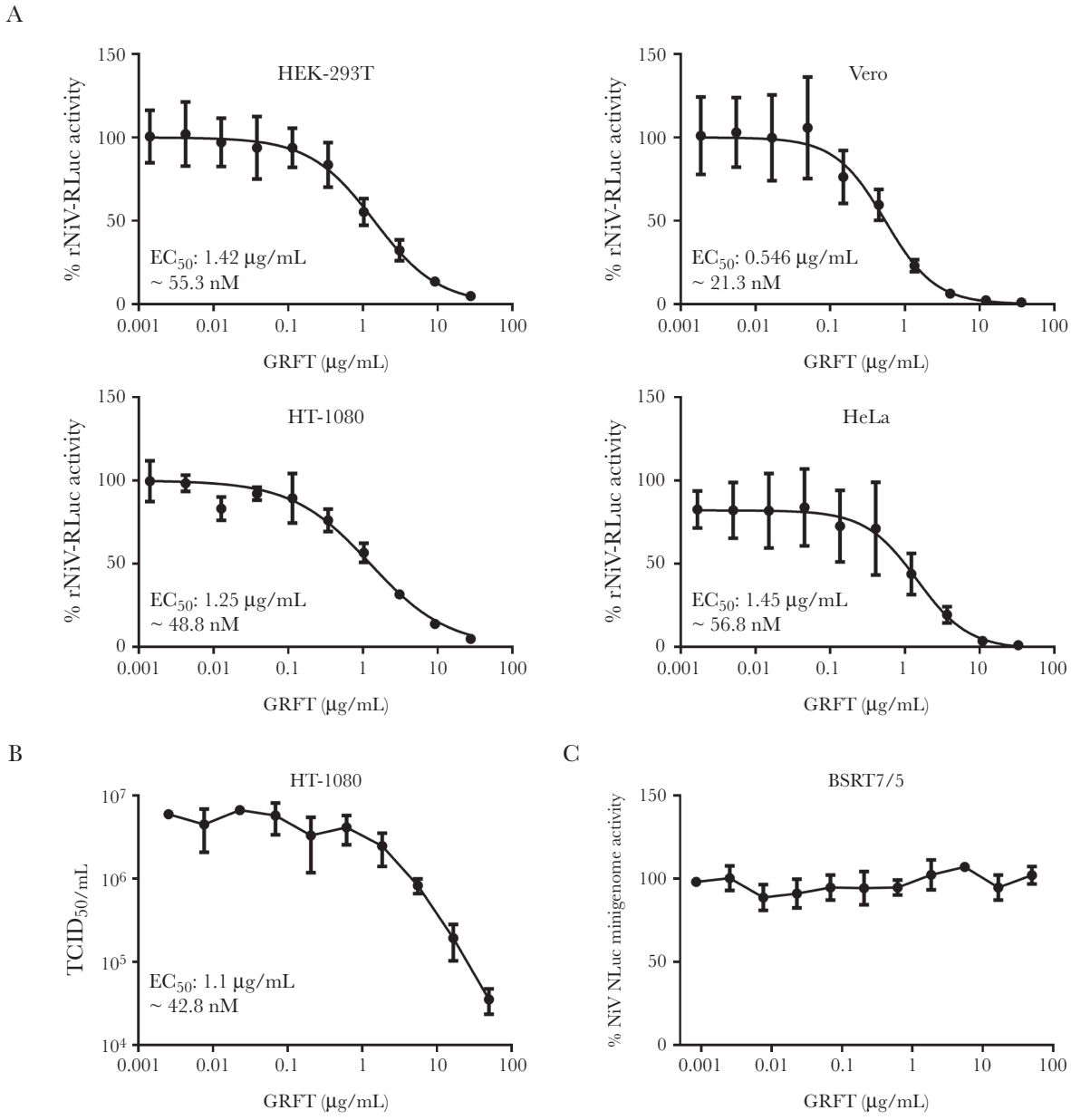

Figure 1. Griffithsin (GRFT) inhibits Nipah virus (NiV) replication but does not inhibit NiV minigenome ribonucleic acid transcription and replication. (*A*) Griffithsin inhibits reporter NiV expressing *Renilla* luciferase (rNiV-RLuc) in human embryonic kidney (HEK-293T), fibrosarcoma (HT-1080), cervical carcinoma (HeLa), and African green monkey kidney cell lines (Vero). Cells were pretreated with 3-fold serial dilutions of GRFT for 1 hour before being infected with rNiV-RLuc at multiplicity of infection (MOI) of 0.25. At 24 hours post infection (hpi), *Renilla* luciferase activity was measured and normalized to untreated cells infected with rNiV-RLuc. Fifty percent effective inhibition concentrations (EC_{50}) of GRFT (in µg/mL) are indicated alongside their respective converted molar concentrations. (*B*) GRFT reduces NiV infectious yield. HT-1080 cells were infected with recombinant wild-type NiV (Malaysian strain, NiV-M) at an MOI of 0.25 for 1 hour. After removal of NiV inoculum, cells were washed once with phosphate-buffered saline and replenished with growth media. At 24 hpi, cell supernatants were harvested and subjected to 10-fold serial dilutions to inoculate Vero cells to assess virus yield by 50% tissue culture infectious dose ($TCID_{50}$) assay. (*C*) GRFT does not inhibit NiV minigenome activity. BSRT7/5 cells were transfected for 4 hours with plasmids encoding the NiV nucleoprotein (NiV N), phosphoprotein (NiV P), polymerase (NiV L), and the NiV nanoluciferase (NLuc) expressing minigenome. After 4 hours, transfection mixtures were removed from cells and replenished with growth media containing 3-fold dilutions of GRFT. At 48 hours posttransfection, NLuc activity was measured and normalized to untreated cells. Dose-response experiments against rNiV-RLuc were performed in quadruplicate for each concentration in at least 2 independent experiments for each cell line except for HEK-293T. Infectious yield experiment was performed once in quadruplicate for each concentration of GRFT. Minigenome experiment was performed once in triplicate for each concentration of GRFT.

GRFT Blocks NiV Entry and Spread via Interactions With Viral and Cellular Glycoproteins

Because GRFT preferably binds to high mannose N-linked oligosaccharides found commonly on viral envelope glycoproteins [39, 40], we sought to characterize the interaction of GRFT with purified NiV-M fusion (NiV-F AU1) and attachment

Table 1. Summary of GRFT and 3mG In Vitro Antiviral Activity

Virus Family	Virus ID	Genotype/Strain	Assay Type	EC_{50} (nM)	
				GRFT	3mG
Paramyxoviridae	NiV	M (Malaysia)	VTR	42.8	ND
			CPE	81.3 ± 26.7	29.4
	NiV	B (Bangladesh)	VTR	116.5	30.6
			CPE	20.9 ± 0.37	10.4 ± 0.14
	NiV	M-rNiV-RLuc	REP	49.6 ± 19.9	8.4 ± 2.0
	NiV	M-rNiV-ZsG	VTR	138.4	32.1
	HeV	1996	CPE	49.3 ± 12.4	16.8 ± 2.9
	MV	$rMV^{EZ}GFP(3)$	REP	NI	NI
	MuV	rMuV-GFP (IA-2006)	REP	0.33 ± 0.033	3.7 ± 0.23
	hPIV3	JS-GFP	REP	271.7 ± 8.0	18.5 ± 0.25
Pneumoviridae	hMPV	CAN97-83-GFP	REP	NI	NI
Arenaviridae	LASV	Josiah-ZsG	REP	NI	NI
Bunyaviridae	CCHFV	Ibar10200-ZsG	REP	NI	72.9 ± 48.7

Abbreviations: CCHFV, Crimean-Congo hemorrhagic fever virus; CPE, cytopathic effect; EC_{50}, 50% effective concentration; GRFT, griffithsin; HeV, Hendra virus; hMPV, human metapneumovirus; hPIV3, human parainfluenza virus 3; ID, identification; LASV, Lassa virus; MuV, mumps virus; MV, measles vaccine virus; ND, not done; NI, no inhibition; NiV, Nipah virus; REP, reporter assay; VTR, virus titer reduction; 3mG, synthetic trimeric tandemer.

(NiV-G His6×) surface glycoproteins (Supplemental Figure S1A–C). We used GRFT to probe against NiV-F AU1 and NiV-G His6× by Western blot, and we detected both proteins (Figure 2A, left panel, well no. 6 NiV-F AU1, well no. 10 NiV-G). To further characterize these interactions, we performed ELISA binding assays by titrating increasing levels of GRFT against the purified glycoproteins, and we observed comparatively greater binding to NiV-G than to NiV-F (Figure 2A, right panel). We then conducted time-of-addition experiments to determine how long after infection could GRFT still inhibit virus replication. We either incubated serial dilutions of GRFT with rNiV-RLuc for 2 hours before infection or added GRFT at 0, 2, 6, or 12 hpi. Although a 2-hour pre-incubation of GRFT with rNiV-RLuc showed negligible differences in inhibition compared with GRFT treatment at 0 hpi, gradually increasing reporter activity correlated with longer delays before GRFT treatment (Figure 2B, left panel). It is notable, however, that even when GRFT was added 12 hpi, at concentrations of ≥~40 nM GRFT reporter activity was still reduced compared with untreated control infected cells. Dose-response curves for reporter activity indicated an approximately 5- to 6-fold decrease in potency between 0 and 12 hpi treatments, with GRFT treatments at 2 or 6 hpi showing an intermediate 2- to 3-fold comparative decrease to 0 hpi treatment (Figure 2B, right panel).

To determine whether GRFT inhibition of NiV could be overcome by more virus, we used increasing amounts of rNiV-RLuc to infect GRFT-pretreated cells. We observed a dose-dependent increase in reporter activity against ~40 nM of GRFT in 2 cell types, but at higher concentrations of GRFT (~120–360 nM), there were only minimal increases in reporter signal (Figure 2C, left and right panels). This indicated that higher concentrations of GRFT may better inhibit NiV entry and spread indirectly via binding to cellular glycoproteins.

To visualize GRFT-mediated inhibition of NiV spread, we performed immune fluorescence assay of cells infected with rNiV before treatment with GRFT. In untreated infected cells, we observed large holes in the cell monolayer caused by NiV-induced syncytia, with widespread NiV nucleoprotein antigen present (Figure 2D, top leftmost panel). With increasing amounts of GRFT, we observed smaller syncytia concomitant with a visible decrease in infected cells (Figure 2D, top 3 right panels). Cells treated with GRFT were positively stained with an anti-GRFT polyclonal antibody, indicating GRFT binding to cell-surface glycoproteins (Figure 2D, bottom 3 right panels).

Trimeric GRFT Tandemer Has Enhanced Potency Against NiV

The presence of more than 1 oligosaccharide-binding face in the dimeric form of GRFT is crucial to maintain its potent anti-HIV-1 activity [41, 42]. Several synthetically linked tandemers of mGRFT have shown up to 10-fold greater in vitro potency than GRFT [20]. We compared the antiviral activities of GRFT to mGRFT, to a synthetic dimer (2mG), a synthetic trimer (3mG), and a Q-GRFT containing 1 amino acid change (M78→Q), and we found that 3mG was most potent, Q-GRFT was equivalently potent, 2mG was less potent, and that mGRFT had lost all antiviral activity against rNiV-RLuc (Figure 3A, left and right panels, Table 1). To confirm these findings, we tested GRFT, 2mG, 3mG, and Q-GRFT against wild-type NiV-B, NiV-M, and HeV, and we observed similar trends as seen for rNiV-RLuc, with 3mG having the greatest antiviral potency (Figure 3B, Table 1). Among these compounds, only 3mG showed mild cytotoxicity at higher concentrations. We also observed varied antiviral potencies for GRFT and 3mG against other respiratory and hemorrhagic fever viruses of human public health importance, ranging from no activity to potent activity with sub-nanomolar EC_{50} values (Table 1, Supplementary Figures S2A–D and S3A and B).

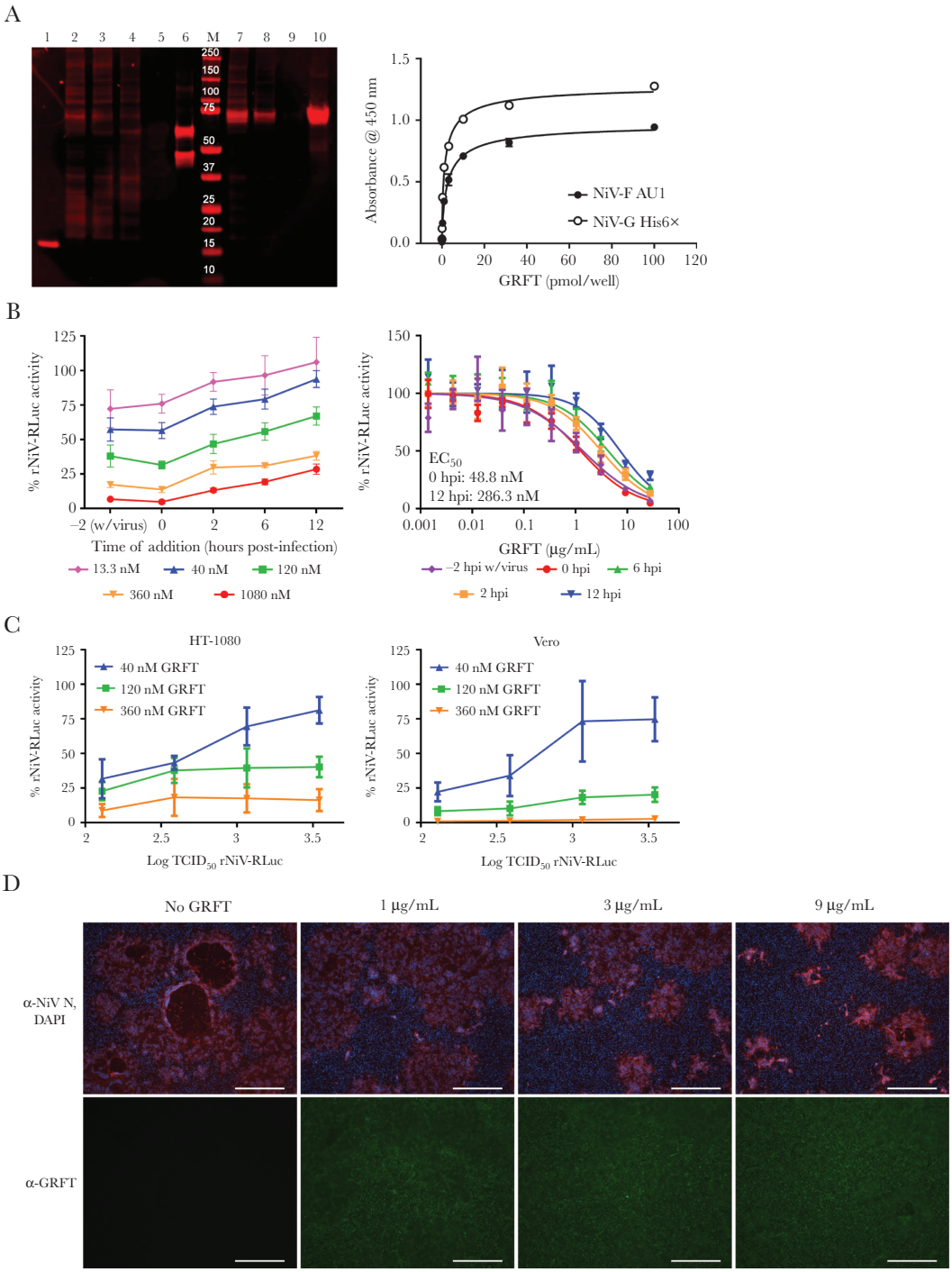

Figure 2. GRFT inhibits NiV entry and spread by its interaction with both NiV Malaysia (NiV-M) and cellular glycoproteins. (*A*) (Left panel) Western blot probed with GRFT and detected with anti-GRFT antibodies + LI-COR imaging. (Lane ID) (1) 100 ng of His-tagged GRFT; (2) 20 µg of mCherry-transfected HEK-293T lysate; (3) 20 µg of NiV-F AU1-transfected HEK-293T lysate; (4) 20 µg of NiV-F anti-AU1 bead flow through; (5) NiV anti-AU1 bead wash; (6) 200 ng of affinity-purified NiV-F AU1; (M) dual color molecular weight standard; (7) 20 µg of NiV-G His6×-transfected HEK-293T lysate; (8) 20 µg of NiV-G His6× NiNTA flow through; (9) NiV-G His6× NiNTA wash; (10) 1 µg of affinity-purified NiV-G His6×. (Right panel) Enzyme-linked immunosorbent assay. Data are representative of 3 experiments in triplicate. (*B*) Time of addition reporter rNiV-RLuc assay. (Left panel) RNiV-RLuc activity measured from infected HT-1080 cells treated with various concentrations of GRFT at indicated times on x-axis. (Right panel) Dose-response curves of rNiV-RLuc activity plotted against GRFT concentration. Effective inhibition concentrations (EC_{50}) for rNiV-RLuc activity for GRFT treatment at 0 and 12 hours post infection are indicated. (*C*) Increasing levels of rNiV-RLuc infection can partially overcome GRFT inhibition at suboptimal concentrations. HT-1080 (left panel) and Vero (right panel) cells were pretreated with GRFT for 1 hour and then infected with increasing levels of rNiV-RLuc. *Renilla* luciferase activity was normalized to activity measured in untreated infected cells. (*D*) Griffithsin inhibits rNiV spread in HT-1080 cells. Immune fluorescence assay. Cells were infected with wild-type rNiV for 1 hour before treatment with GRFT. Cells were fixed in 10% formalin and stained with anti-NiV nucleoprotein (NiV N) mouse monoclonal and anti-GRFT rabbit polyclonal antibodies, and, respectively, detected with Dylight550 (red stain; top panels) and Dylight488 (green stain; bottom panels) secondary detection antibodies, with cell nuclei being stained with 4′,6-diamidino-2-phenylindole (DAPI). White bars indicate 500 microns in length. Reporter rNiV-RLuc assays were performed once in triplicate.

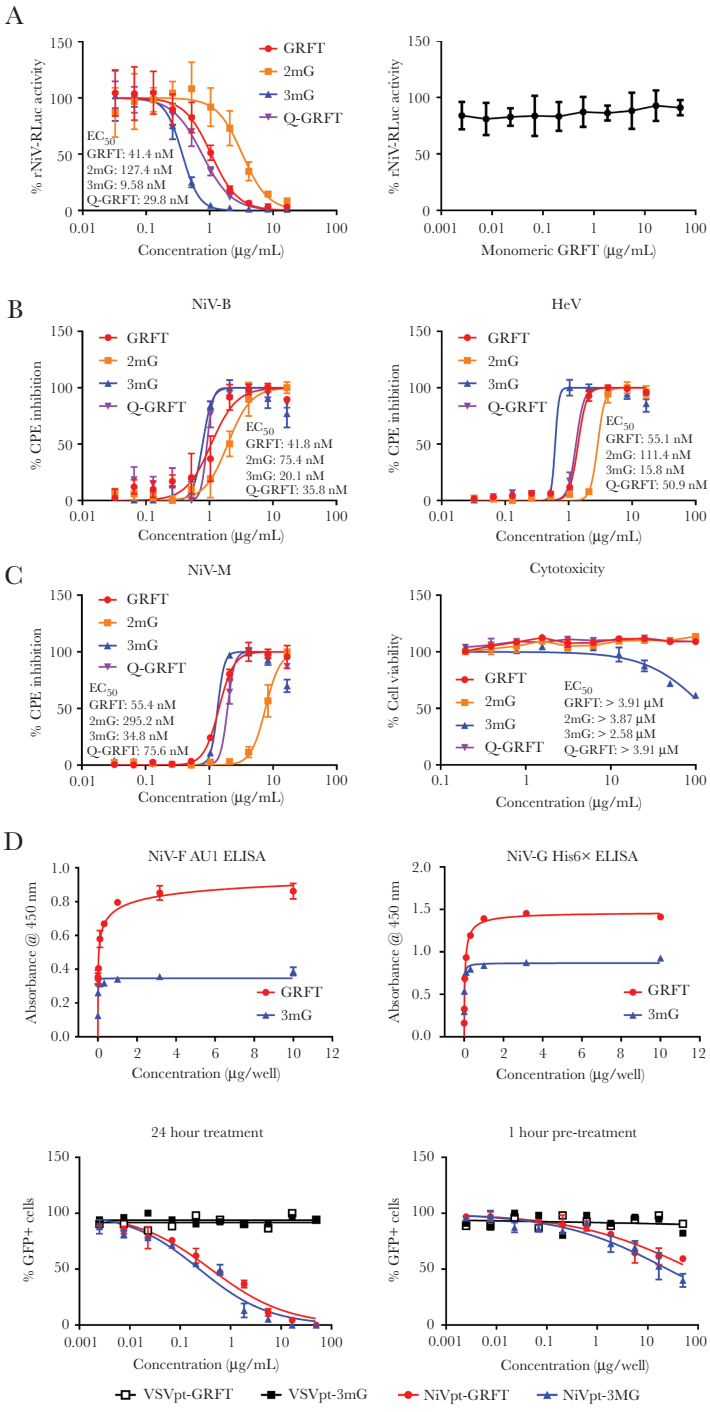

Figure 3. Synthetic monomeric tandemers of GRFT show variable activities to bind purified NiV glycoproteins and to block against Henipavirus cytopathic effect (CPE) and entry. (*A*) (Left panel) Trimeric monomer of GRFT (3mG) blocks reporter rNiV-RLuc activity more efficiently than GRFT and a synthetic dimeric monomer of GRFT (2mG). (Right panel) Inhibition of rNiV-RLuc is ablated against the monomeric GRFT. (*B*) The 3mG shows enhanced ability to block CPEs from NiV Bangladesh (NiV-B), NiV Malaysia (NiV-M), and HeV infection over GRFT, oxidation-resistant (Q-GRFT), and 2mG. Vero cells pretreated with either GRFT, 2mG, 3mG, or Q-GRFT were either infected with NiV-B (top left panel), HeV (top right panel), or NiV-M (bottom left panel) (multiplicity of infection = 0.25) or mock infected (bottom right panel) for 72 hours and were assayed for cell viability using CellTiterGlo 2.0 reagent as a measure of CPE inhibition. Levels of CPE were normalized to cell viability of uninfected cells. (*C*) Binding enzyme-linked immunosorbent assay (ELISA). The 3mG shows comparatively less binding as GRFT to purified NiV glycoproteins. Half-log serial dilutions of GRFT (red circles) and 3mG (blue triangles) were incubated with immobilized purified Malaysian NiV-F AU1 glycoprotein (left panel) or NiV-G His6× attachment glycoprotein (right panel) and detected by an anti-GRFT rabbit polyclonal antibody and an antirabbit horseradish peroxidase-conjugated antibody. Absorbance levels at 450 nm indicate levels of binding as plotted against increasing concentrations of GRFT or 3mG on the x-axis. (*D*) GRFT and 3mG equivalently block NiV-F- and NiV-G-pseudotyped vesicular stomatitis virus (VSV) replication-deficient particles expressing enhanced green fluorescent protein (GFP). Vero cells were treated with 3-fold serial dilutions of GRFT or 3mG for 24 hours (left panel) concurrently with infection or pretreated for 1 hour (right panel) before infection with replication-deficient VSV particles pseudotyped either with VSV-G glycoprotein (VSVpt) or the NiV-F and NiV-G glycoproteins (NiVpt). At 24 hours postinfection, numbers of GFP-positive infected cells were counted and normalized to numbers from untreated infected cells. Reporter rNiV-RLuc assays were performed once in triplicate, CPE assays were performed at least twice in triplicate, ELISAs were performed at least twice in triplicate, and pseudotyped experiments were performed twice in duplicate at each respective concentration of GRFT and 3mG.

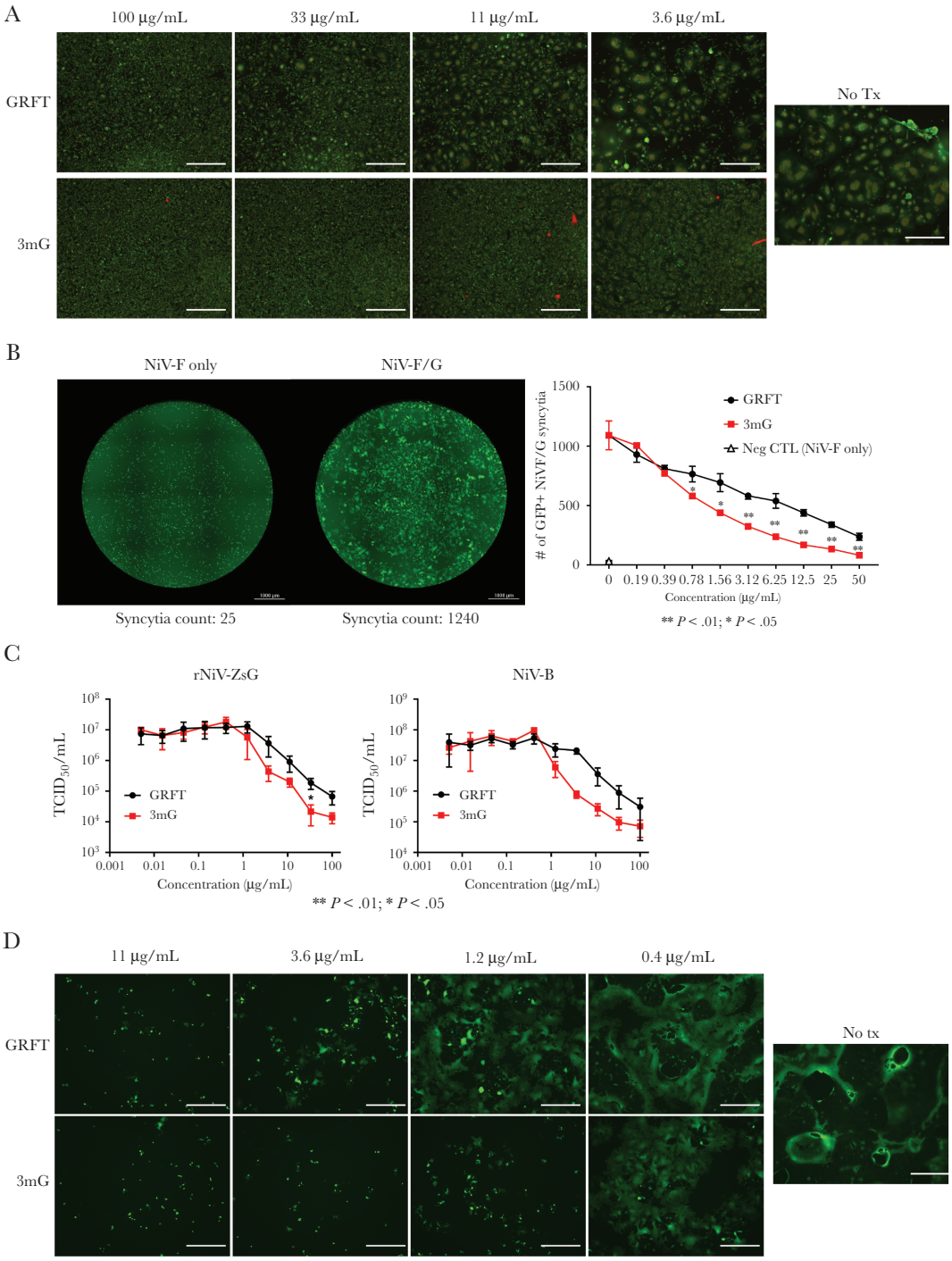

Figure 4. The superior ability of trimeric monomer of griffithsin ([GRFT] 3mG) over GRFT to block NiV glycoprotein-mediated syncytia formation is mirrored by its enhanced reduction of NiV infectious yield. (*A*) Fusion assay. HT-1080 cells transfected with NiV-F and NiV-G expression plasmids were (1) treated with 3-fold dilutions of either GRFT (top panels) or 3mG (bottom panels) for 16 hours, (2) fixed and stained with CellMask Green (green cytoplasmic stain) and 4',6-diamidino-2-phenylindole (colored red for contrast), and (3) observed for syncytia formation. "No Tx" indicates transfected cells not treated with either GRFT or 3mG. White bars indicate 500 microns. (*B*) Quantitative image-based syncytia counting assay. Fluorescent micrograph montages (left panel) were created of individual wells of CHO-K1 cells transfected with NiV-F plasmid only or with both NiV-F and NiV-G plasmids, overlaid with bacteriophage T7 polymerase expressing BSRT7/5 cells, with syncytia counts indicated for each respective well. Numbers of green fluorescent protein (GFP)-positive NiV glycoprotein- induced syncytia are plotted against increasing concentrations of either GRFT (black circles) or 3mG (red squares) (right panel). Adjusted *P* values for multiple *t* tests performed to compare numbers of syncytia between GRFT and 3mG-treated cells at each concentration are indicated by single or double asterisks. (*C*) The 3mG more efficiently reduces infectious virus yield compared with GRFT. Vero cells were infected with either reporter NiV expressing ZsGreen protein (rNiV-ZsG) (left panel) or NiV Bangladesh (NiV-B) (right panel) (multiplicity of infection = 0.25) for 1 hour before being treated with 2-fold serial dilutions of GRFT (black circles) or 3mG (red squares). At 48 hours post infection, infectious yield was measured using 50% tissue culture infectious dose ($TCID_{50}$) assay and was plotted against respective compound concentrations. (*D*) Fluorescent micrographs of rNiV-ZsG-infected Vero cells treated with various dilutions of either GRFT or 3mG. "No tx" indicates untreated infected cells. White bar indicates 500 microns.

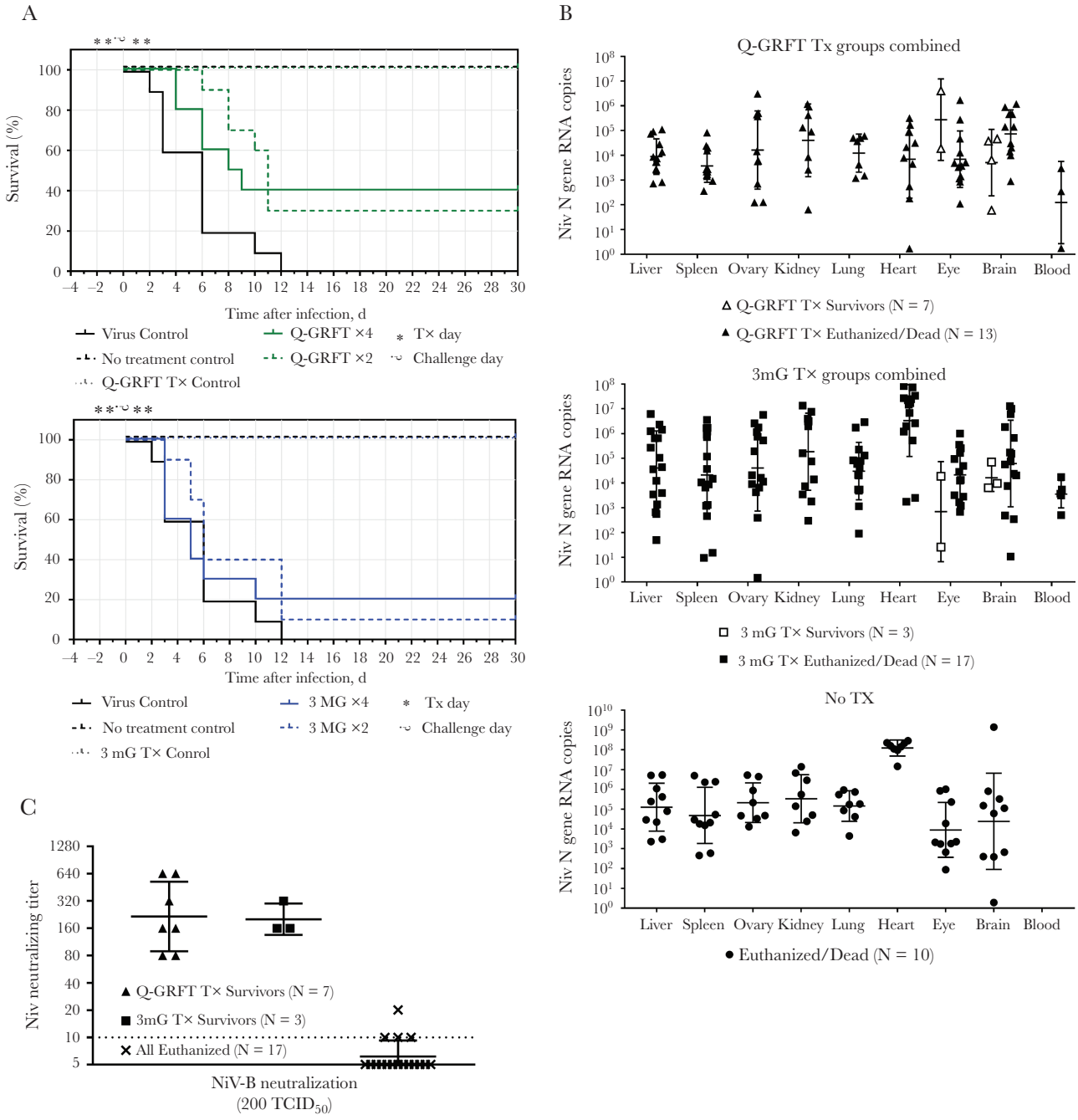

Figure 5. Prophylactic intranasal administration of oxidation-resistant griffithsin (Q-GRFT) provides significant protection from lethal intranasal NiV-B challenge. (*A*) Survival curves for animals treated with either 2× or 4× doses of Q-GRFT (top panel, green lines) or trimeric monomer of GRFT ([3mG] bottom panel, blue lines). The Q-GRFT and 3mG Tx control animals were not infected with NiV-B. Asterisks indicate treatment days, whereas rotated question mark indicates day of virus challenge. Animal survival curves were analyzed by log-rank (Mantel-Cox) and Gehan-Breslow-Wilcoxon test and were significantly different by both tests, with $P < .0001$. (*B*) NiV nucleoprotein (NiV N) gene RNA copy numbers (normalized to 18S ribosomal RNA) in various tissues and blood of animals treated with Q-GRFT (top panel), 3mG (middle panel), or untreated animals (bottom panel). Geometric mean for each tissue is indicated by horizontal lines bisecting the error bars. (*C*) Virus neutralization assay. $TCID_{50}$ of NiV-B was incubated in duplicate with 2-fold dilutions of animal sera for 1 hour before being overlaid onto Vero cells for 6 days. The highest reciprocal dilution at which both wells were free of cytopathic effect was recorded as the NiV-neutralizing titer. Geometric means are indicated by horizontal lines bisecting the error bars.

To understand the greater in vitro activity of 3mG compared with GRFT, we performed ELISA protein binding assays against purified NiV-M F and G glycoproteins. We observed greater binding by GRFT to both glycoproteins than by 3mG, which was contrary to their virus inhibition profiles (Figure 3C). We then compared the abilities of GRFT and 3mG to block virus entry by

replication-deficient, eGFP-expressing VSVs pseudotyped with either the VSV G glycoprotein (VSVpt) or with both NiV-M F and G glycoproteins (NiVpt). We did not observe significant differences in antiviral potencies at equivalent compound concentrations under both continuous GRFT/3mG treatment or with only 1 hour of pretreatment before infection (Figure 3D, left and right panels, respectively).

3mG More Efficiently Reduces Syncytia Formation and Infectious Yield

We tested the abilities of GRFT and 3mG to block NiV-F and NiV-G glycoprotein-induced syncytia formation by treating transfected cells expressing both NiV-F and NiV-G glycoproteins with either compound, and we observed that 3mG visibly inhibited syncytia formation more efficiently than GRFT at equivalent concentrations (Figure 4A). To confirm this result, we developed a quantitative image-based syncytia counting assay. Whereas cells transfected only with NiV-F plasmid had minimal background syncytia counts, cells transfected with both NiV glycoproteins had >1000 syncytia counts (Figure 4B, left panel). Using this assay, we observed a dose-dependent decrease in syncytia counts that correlated with increased levels of GRFT or 3mG, but we noted that 3mG more efficiently reduced syncytia than GRFT at higher concentrations (Figure 4B, right panel). When Vero cells were treated with GRFT or 3mG after infection by either green fluorescent reporter NiV (rNiV-ZsG) or NiV-B, 3mG reduced virus yield more efficiently than GRFT, similarly reflecting their differing abilities to block syncytia formation (Figure 4C, left and right panels, respectively). Accordingly, 3mG visibly delayed or reduced the size of syncytia formation more efficiently than GRFT in rNiV-ZsG infected cells (Figure 4D).

Q-GRFT Can Protect Hamsters From Lethal Nipah Virus-B Challenge

Finally, we explored the in vivo prophylactic potential of 3mG and of the Q-GRFT [21] against a uniformly lethal intranasal challenge dose of NiV-B (~10^7 $TCID_{50}$) in Syrian golden hamsters [43]. Groups of 10 animals each received intranasal doses of either Q-GRFT (10 mg/kg), 3mG (10 mg/kg) on days 1 and 2 before challenge (for 2× dose and 4× dose treatment groups), and on days 1 and 2 post challenge (for 4× dose treatment groups only). Vehicle control animals received an intranasal equivalent dose volume of PBS on the same 4 treatment days as the 4× dose treatment groups. Animals receiving either 2 or 4 doses of Q-GRFT treatment groups showed partial but significant protection from NiV-B challenge (~35% survival rate across Q-GRFT treatment groups) (Figure 5A, top panel), whereas only 3 animals across 3mG treatment groups survived infection (~15% overall survival rate) (Figure 5A, bottom panel). More than 70% of Q-GRFT treated survivors had no clinical signs by the end of the study, whereas only one 3mG treated survivor lacked clinical signs (Supplemental Figure S4C). Nipah virus RNA was detected in most tissues sampled from euthanized or dead animals (Figure 5B, filled shapes in all 3 panels), but it was only detected in the eyes and brains of Q-GRFT and 3mG treated survivors (Figure 5B, open triangles and squares in top 2 panels). All survivors from Q-GRFT and 3mG treatment groups developed neutralizing antibody titers against NiV (Figure 5C, Supplemental Table).

DISCUSSION

In this study, we characterized the in vitro antiviral activity of GRFT and its 3mG tandemer against NiV and a series of other important human viral pathogens. Similar to in vitro observations for HIV-1, GRFT and 3mG can block both NiV entry and cell-to-cell spread [15, 20]. Although 3mG consistently outperformed GRFT in its ability to block both NiV glycoprotein-induced cell-to-cell fusion and NiV infectious yield, it had comparatively weaker ELISA binding profiles against purified NiV glycoproteins. This observation could be explained by differences in anti-GRFT polyclonal antibody binding to 3mG because it is not an obligate dimer as is wild-type GRFT, against which the polyclonal antibodies were generated. Future biochemical and structural studies should not only identify the N-glycosylation sites on NiV-F and NiV-G that are important for antiviral susceptibility to GRFT/3mG, but also investigate the molecular interactions of GRFT/3mG with NiV-F and NiV-G proteins to determine how these may alter the biophysical properties of a NiV virion. Despite the superior in vitro ability of 3mG to block NiV syncytia formation and virus yield, 3mG protected less than half as many animals as did Q-GRFT from in vivo challenge. This can be attributed to 3mG likely having a shorter in vivo half-life compared with Q-GRFT, which is significantly more resistant to oxidation compared with wild-type GRFT [21]. The 3mG may require re-engineering to achieve better in vivo efficacy, because 3mG contains flexible linkers that are more susceptible to proteolytic cleavage than GRFT [44]. Although all survivors developed significant neutralizing antibodies against NiV, only 1 survivor treated with 3mG tested positive for total anti-NiV IgG (Supplemental Table), suggesting that the majority of NiV-specific antibodies generated in Q-GRFT/3mG-treated survivors target the surface glycoproteins. The GRFT and other lectins represent another avenue towards developing NiV therapeutics. Because NiV glycoprotein glycosylation modulates syncytia formation and shields against neutralizing antibodies [45, 46], retaining these glycosylation sites likely maintains viral fitness. A potential treatment regimen combining GRFT with both monoclonal antibody m102.4 and nucleotide prodrug remdesivir would provide an additional constraint against development of NiV escape mutants.

CONCLUSIONS

Our findings, taken together with the favorable pharmacokinetic and safety profiles of GRFT [22, 47–49], make Q-GRFT

an excellent candidate for further preclinical evaluation against NiV infection.

Supplementary Data

Supplementary materials are available at *The Journal of Infectious Diseases* online. Consisting of data provided by the authors to benefit the reader, the posted materials are not copyedited and are the sole responsibility of the authors, so questions or comments should be addressed to the corresponding author.

Notes

Acknowledgments. We thank Tatyana Klimova for assistance with editing the manuscript. We thank Jennifer Wilson (National Cancer Institute) for antiviral activity testing.

Disclaimer. The content of this publication does not necessarily reflect the views or policies of the Department of Health and Human Services, nor does mention of trade names, commercial products, or organizations imply endorsement by the U.S. Government. The findings and conclusions in this report are those of the authors and do not necessarily represent the official position of the Centers for Disease Control and Prevention.

Financial support. This work was partially funded by an appointment to the Research Participation Program at the Centers for Disease Control and Prevention (CDC) administered by the Oak Ridge Institute for Science and Education through an interagency agreement between the US Department of Energy and CDC (to S. R. W.) and by CDC Emerging Infectious Disease Research Core Funds. This project has been funded in whole or in part with federal funds from the National Cancer Institute, National Institutes of Health, under contract HHSN26120080001E. This research was also supported in part by the Intramural Research Program of the National Institutes of Health (NIH), National Cancer Institute, Center for Cancer Research. This work was also supported in part by funds from the NIH Intramural AIDS Targeted Antiviral Program and Center for Cancer Research at the National Cancer Institute (to B. R. O.).

Potential conflicts of interest. B. R. O. and K. E. P. are listed as inventors on patents owned by the US Government on GRFT, Q-GRFT, and GRFT-tandemers. All authors have submitted the ICMJE Form for Disclosure of Potential Conflicts of Interest. Conflicts that the editors consider relevant to the content of the manuscript have been disclosed.

References

1. Spiropoulou CF. Nipah virus outbreaks: still small but extremely lethal. J Infect Dis **2019**; 219:1855–7.
2. Lo MK, Feldmann F, Gary JM, et al. Remdesivir (GS-5734) protects African green monkeys from Nipah virus challenge. Sci Transl Med **2019**; 11:eaau9242.
3. Mire CE, Satterfield BA, Geisbert JB, et al. Pathogenic differences between Nipah virus Bangladesh and Malaysia strains in primates: implications for antibody therapy. Sci Rep **2016**; 6:30916.
4. Dawes BE, Kalveram B, Ikegami T, et al. Favipiravir (T-705) protects against Nipah virus infection in the hamster model. Sci Rep **2018**; 8:7604.
5. Xu K, Rockx B, Xie Y, et al. Crystal structure of the Hendra virus attachment G glycoprotein bound to a potent cross-reactive neutralizing human monoclonal antibody. PLoS Pathog **2013**; 9:e1003684.
6. Mathieu C, Porotto M, Figueira TN, Horvat B, Moscona A. Fusion inhibitory lipopeptides engineered for prophylaxis of Nipah virus in primates. J Infect Dis **2018**; 218:218–27.
7. Mathieu C, Augusto MT, Niewiesk S, et al. Broad spectrum antiviral activity for paramyxoviruses is modulated by biophysical properties of fusion inhibitory peptides. Sci Rep **2017**; 7:43610.
8. Niedermeier S, Singethan K, Rohrer SG, et al. A small-molecule inhibitor of Nipah virus envelope protein-mediated membrane fusion. J Med Chem **2009**; 52:4257–65.
9. Bossart KN, Mungall BA, Crameri G, Wang LF, Eaton BT, Broder CC. Inhibition of Henipavirus fusion and infection by heptad-derived peptides of the Nipah virus fusion glycoprotein. Virol J **2005**; 2:57.
10. Mathieu C, Dhondt KP, Châlons M, et al. Heparan sulfate-dependent enhancement of henipavirus infection. MBio **2015**; 6:e02427.
11. Garner OB, Yun T, Pernet O, et al. Timing of galectin-1 exposure differentially modulates Nipah virus entry and syncytium formation in endothelial cells. J Virol **2015**; 89:2520–9.
12. Garner OB, Aguilar HC, Fulcher JA, et al. Endothelial galectin-1 binds to specific glycans on Nipah virus fusion protein and inhibits maturation, mobility, and function to block syncytia formation. PLoS Pathog **2010**; 6:e1000993.
13. Levroney EL, Aguilar HC, Fulcher JA, et al. Novel innate immune functions for galectin-1: galectin-1 inhibits cell fusion by Nipah virus envelope glycoproteins and augments dendritic cell secretion of proinflammatory cytokines. J Immunol **2005**; 175:413–20.
14. Clinicaltrials.gov. Available at: https://clinicaltrials.gov/ct2/results?cond=&term=griffithsin&cntry=&state=&city=&dist=.
15. Mori T, O'Keefe BR, Sowder RC 2nd, et al. Isolation and characterization of griffithsin, a novel HIV-inactivating protein, from the red alga Griffithsia sp. J Biol Chem **2005**; 280:9345–53.
16. Kouokam JC, Lasnik AB, Palmer KE. Studies in a murine model confirm the safety of griffithsin and advocate its further development as a microbicide targeting HIV-1 and other enveloped viruses. Viruses **2016**; 8:E311.
17. Ishag HZ, Li C, Huang L, et al. Griffithsin inhibits Japanese encephalitis virus infection in vitro and in vivo. Arch Virol **2013**; 158:349–58.
18. O'Keefe BR, Giomarelli B, Barnard DL, et al. Broad-spectrum in vitro activity and in vivo efficacy of the

antiviral protein Griffithsin against emerging viruses of the family *Coronaviridae*. J Virol **2010**; 84:2511–21.
19. Takebe Y, Saucedo CJ, Lund G, et al. Antiviral lectins from red and blue-green algae show potent in vitro and in vivo activity against hepatitis C virus. PLoS One **2013**; 8:e64449.
20. Moulaei T, Alexandre KB, Shenoy SR, et al. Griffithsin tandemers: flexible and potent lectin inhibitors of the human immunodeficiency virus. Retrovirology **2015**; 12:6.
21. O'Keefe BR, Moulaei T, Palmer KE, Rohan LC, Fuqua JL, Kramzer LF, inventors; The United States of America, as represented by the Secretary, Department of Health and Human Services, University of Louisville Research Foundation, Inc., University of Pittsburgh - Of the Commonwealth System of Higher Education, assignees. Griffithsin mutants. US patent; 18 January 2018. Patent application number: 20180016307.
22. O'Keefe BR, Vojdani F, Buffa V, et al. Scaleable manufacture of HIV-1 entry inhibitor griffithsin and validation of its safety and efficacy as a topical microbicide component. Proc Natl Acad Sci U S A **2009**; 106:6099–104.
23. Fuqua JL, Wanga V, Palmer KE. Improving the large scale purification of the HIV microbicide, griffithsin. BMC Biotechnol **2015**; 15:12.
24. Buchholz UJ, Finke S, Conzelmann KK. Generation of bovine respiratory syncytial virus (BRSV) from cDNA: BRSV NS2 is not essential for virus replication in tissue culture, and the human RSV leader region acts as a functional BRSV genome promoter. J Virol **1999**; 73:251–9.
25. Lo MK, Jordan R, Arvey A, et al. GS-5734 and its parent nucleoside analog inhibit Filo-, Pneumo-, and Paramyxoviruses. Sci Rep **2017**; 7:43395.
26. Mohr EL, McMullan LK, Lo MK, et al. Inhibitors of cellular kinases with broad-spectrum antiviral activity for hemorrhagic fever viruses. Antiviral Res **2015**; 120:40–7.
27. Lo MK, Nichol ST, Spiropoulou CF. Evaluation of luciferase and GFP-expressing Nipah viruses for rapid quantitative antiviral screening. Antiviral Res **2014**; 106:53–60.
28. Rennick LJ, de Vries RD, Carsillo TJ, et al. Live-attenuated measles virus vaccine targets dendritic cells and macrophages in muscle of nonhuman primates. J Virol **2015**; 89:2192–200.
29. Xu P, Li Z, Sun D, et al. Rescue of wild-type mumps virus from a strain associated with recent outbreaks helps to define the role of the SH ORF in the pathogenesis of mumps virus. Virology **2011**; 417:126–36.
30. Zhang L, Bukreyev A, Thompson CI, et al. Infection of ciliated cells by human parainfluenza virus type 3 in an in vitro model of human airway epithelium. J Virol **2005**; 79:1113–24.
31. Biacchesi S, Skiadopoulos MH, Tran KC, Murphy BR, Collins PL, Buchholz UJ. Recovery of human metapneumovirus from cDNA: optimization of growth in vitro and expression of additional genes. Virology **2004**; 321:247–59.
32. Welch SR, Guerrero LW, Chakrabarti AK, et al. Lassa and Ebola virus inhibitors identified using minigenome and recombinant virus reporter systems. Antiviral Res **2016**; 136:9–18.
33. Welch SR, Scholte FE, Flint M, et al. Identification of 2'-deoxy-2'-fluorocytidine as a potent inhibitor of Crimean-Congo hemorrhagic fever virus replication using a recombinant fluorescent reporter virus. Antiviral Res **2017**; 147:91–9.
34. Reed LJ, Muench H. A simple method of estimating fifty percent endpoints. Am J Hygiene **1938**; 27:493–7.
35. Hotard AL, He B, Nichol ST, Spiropoulou CF, Lo MK. 4'-Azidocytidine (R1479) inhibits henipaviruses and other paramyxoviruses with high potency. Antiviral Res **2017**; 144:147–52.
36. Chiang CF, Lo MK, Rota PA, Spiropoulou CF, Rollin PE. Use of monoclonal antibodies against Hendra and Nipah viruses in an antigen capture ELISA. Virol J **2010**; 7:115.
37. Chattopadhyay A, Rose JK. Complementing defective viruses that express separate paramyxovirus glycoproteins provide a new vaccine vector approach. J Virol **2011**; 85:2004–11.
38. Lo MK, Lowe L, Hummel KB, et al. Characterization of Nipah virus from outbreaks in Bangladesh, 2008–2010. Emerg Infect Dis **2012**; 18:248–55.
39. Ziółkowska NE, Shenoy SR, O'Keefe BR, et al. Crystallographic, thermodynamic, and molecular modeling studies of the mode of binding of oligosaccharides to the potent antiviral protein griffithsin. Proteins **2007**; 67:661–70.
40. Ziółkowska NE, Shenoy SR, O'Keefe BR, Wlodawer A. Crystallographic studies of the complexes of antiviral protein griffithsin with glucose and N-acetylglucosamine. Protein Sci **2007**; 16:1485–9.
41. Moulaei T, Shenoy SR, Giomarelli B, et al. Monomerization of viral entry inhibitor griffithsin elucidates the relationship between multivalent binding to carbohydrates and anti-HIV activity. Structure **2010**; 18:1104–15.
42. Xue J, Hoorelbeke B, Kagiampakis I, Demeler B, Balzarini J, Liwang PJ. The griffithsin dimer is required for high-potency inhibition of HIV-1: evidence for manipulation of the structure of gp120 as part of the griffithsin dimer mechanism. Antimicrob Agents Chemother **2013**; 57:3976–89.
43. de Wit E, Prescott J, Falzarano D, et al. Foodborne transmission of Nipah virus in Syrian hamsters. PLoS Pathog **2014**; 10:e1004001.
44. Moncla BJ, Pryke K, Rohan LC, Graebing PW. Degradation of naturally occurring and engineered antimicrobial peptides by proteases. Adv Biosci Biotechnol **2011**; 2:404–8.
45. Aguilar HC, Matreyek KA, Filone CM, et al. N-glycans on Nipah virus fusion protein protect against neutralization but reduce membrane fusion and viral entry. J Virol **2006**; 80:4878–89.

46. Biering SB, Huang A, Vu AT, et al. N-Glycans on the Nipah virus attachment glycoprotein modulate fusion and viral entry as they protect against antibody neutralization. J Virol **2012**; 86:11991–2002.
47. Barton C, Kouokam JC, Hurst H, Palmer KE. Pharmacokinetics of the antiviral lectin griffithsin administered by different routes indicates multiple potential uses. Viruses **2016**; 8:E331.
48. Barton C, Kouokam JC, Lasnik AB, et al. Activity of and effect of subcutaneous treatment with the broad-spectrum antiviral lectin griffithsin in two laboratory rodent models. Antimicrob Agents Chemother **2014**; 58:120–7.
49. Kouokam JC, Huskens D, Schols D, et al. Investigation of griffithsin's interactions with human cells confirms its outstanding safety and efficacy profile as a microbicide candidate. PLoS One **2011**; 6:e22635.